Effects of Propellant Temperature on Fragmentation in the Plume of a Porous Electrospray Thruster

IEPC-2022-209

Presented at the 37th International Electric Propulsion Conference
Massachusetts Institute of Technology, Cambridge, MA, USA
June 19-23, 2022

S. Dworski[1], C. Ma[2] and C.N. Ryan[3]
University of Southampton, Southampton, Hampshire, SO17 1BJ, United Kingdom

A Porous Electrospray Thruster which uses a heater is presented. Three sets of tests are undertaken on the thruster: Current-Voltage-Temperature , Plume Angle Analysis and Retarding Potential Analysis at a voltage range of 2.20kV to 3.50kV and a temperature range of 25°C to 100°C. Current is found to increase with voltage and temperature, ranging from 3.9 μA to -5.9 μA. The plume angle is found to vary between 10° and 20° and remain unchanged through testing. Retarding Potential Analysis shows the proportion of the current accelerated to the maximum potential increases with temperature and decreases with voltage. Furthermore, a higher proportion of the current is accelerated to maximum potential at 60°C than at any other temperature.

I. Introduction

Due to a large increase in CubeSats in the past decade [1], the utilisation of thrusters on board satellites has increased. Many different types of propulsion systems can be used, however one of the most promising propulsion systems for CubeSats are Porous Electrospray Thrusters (PETs) [2]. Porous Electrospray Thrusters utilise a porous emitter tip to emit either molecular ions or charged droplets using an electrostatic field. These are accelerated to a high velocity allowing for high specific impulses and moderate thrusts.

Some physics of PETs are relatively well understood. The behaviour of the thruster is governed by the electrohydrodynamic phenomena which form due to the surface tension of the propellant forming a meniscus under the influence of a strong electric field [3, 4]. As the electric field is increased, it reaches a critical point where the thruster begins to emit charged particles. It has been found that the behaviour of this emission is strongly governed by the propellant properties of the the thruster [5, 6]. Firstly, as the conductivity of the propellant is increased the thruster emits smaller particles [5]. This promotes increasing the conductivity of the propellant. This has led to room temperature molten salts called ionic liquids being utilised for porous electrospray thrusters so that small species are emitted [7].

One such example of an ionic liquid is 1-ethyl-3 methylimidazolium tetrafluoroborate (EMI-BF4). This is one of the most common ionic liquids used for PETs. The charged particles emitted by such a meniscus are typically small ions, made up of singular ions, which can be cations and anions, or an ion-neutral pair, made up of singular ions bonded via intermolecular forces with a neutral molecule. These are called monomers and dimers respectively. Larger ions are possible, with more neutral molecules per ion, however these will not be considered in this report.

The principal mechanisms behind current emission by such a thruster are well understood, both modelling working has been done using activated process equations [8], using molecular dynamics [9] and many experiments have been undertaken characterising the current, including at the University of Southampton [10–12]. The emitted current has been found to also be a strong function of propellant properties, especially the activation energy, ΔG, of the ions which represents the energy barrier for ion emission.

Another key phenomena is the fragmentation of dimers and larger ions in the plume. Due to the weak intermolecular forces between the ion and neutral pair and the strong electric fields, the ion and neutral pair will break. This is called

[1]PhD Student, Aeronautics & Astronautics, S.Dworski@soton.ac.uk
[2]Postdoctoral Researcher, Aeronautics & Astronautics
[3]Associate Professor, Aeronautics & Astronautics

fragmentation. Fragmentation has been an experimentally well document phenomena, for example Lozano quantified the energy levels an 1-ethyl-3-methylimidazolium bis(triflouromethylsulfonyl)amide (EMI-Im) ionic thruster using Time-of-Flight (TOF) mass spectrometry and Retarding Potential Analysis (RPA) [13]. Ma investigated the energies of a thruster operating on EMI-BF4 [14]. Chong *et al* investigated the energies of the plume of a ceramic emitter thruster using EMI-BF4 [15]. Recently, fragmentation has become a better understood phenomena due to the work of Miller [16], quantifying the fragmentation rates of, amongst other ionic liquids, EMI-BF4. This analysis also showed that propellant properties have a strong effect on fragmentation rates, especially the molecular complexity of the propellant.

One aspect which has not been extensively tested is the propellant temperature effects on the emission and fragmentation of the thruster. The usage of temperature has been used in chemistry to investigate thermodynamic properties of chemicals [17], however has not been extensively utilised in thrusters. Some experiments have been conducted which explore temperature effects. Krejci and Lozano showed that as the temperature increases, the plume becomes more fragmented and the current increases approximately linearly [18]. Miller found that as the propellant temperature increased, the lifetime of a dimer cluster decreased [16]. Gamero-Castaño and Cisquella-Serra found that the plume becomes more ionic when the temperature is increased [19]. Gassend *et al* showed that current also increases linearly with temperature, suggesting a limiting ohmic conduction of charges creating this relationship [20].

Due to the propellant properties having strong effects on the thruster, it is expected that temperature should have significant effects on the thruster's emission. For example, the conductivity of EMI-BF4 increases by a factor of ~ 5 at a change between 25^{o}C and 80^{o}C [21]. An investigation into the temperature effects will provide a fuller understanding of the factors affecting emission and fragmentation within the plume of the thruster. Other studies have demonstrated that the electric field and temperature of the emitted ions has a strong effect on the fragmentation rate [22].

This report covers the work done at the University of Southampton in investigating fundamental physical behaviours of PETs. A single emitter heated thruster called the Heated Porous Electrospray Thruster - 1 emitter (HPET-1) based on previous University of Southampton designs is presented. The experimental apparatus and methodology of current collection, plume angle analysis and retarding potential analysis is also presented. Finally the results for current-voltage-temperature, plume angle and voltage-temperature energy experiments are shown.

II. Thruster Design

The HPET-1 is designed based on previous work at the University of Southampton [12]. To enable rapid development and reliable operation, key features such as emitter geometry, material and manufacturing methods were retained. Firstly, the emitter was manufactured from ROBU P5 borosilicate glass (pore size 1.0 to 1.6 μm). The emitter height was 2 mm with a tip radius of 50 μm. The emitter was manufactured using CNC machining at the University of Southampton Engineering Design & Manufacture Centre (EDMC). The emitter fits within a 4 mm $\times$ 4 mm $\times$ 4 mm cube. A single emitter design was selected to reduce the amount of factors influencing plume properties, with multiple emitters allowing for multiple plumes to impinge on each other possibly affecting the overall plume properties. An extractor made out of AISI 316 stainless steel with an aperture size of diameter 1.00 mm was placed 0.5 mm above the emitter tip.

The emitter is connected to an AISI 316 stainless steel porous reservoir with porosity P0 (pore size 160 to 250 μm). The propellant reservoir had two functions for thruster. Firstly it acted as the main propellant stoarge allowing a larger volume of propellant to be stored and, due to the Laplace pressure effect, produce a mass flow for the emitter. Secondly, it acted as the distal electrode for thruster operation due to its large internal surface area. The emitter voltage was connected to the propellant tank by a bolt coming through the back for the thruster. This bolt applied a force to the propellant tank and the emitter which ensured a tight connection between the emitter and the propellant tank and alignment between the emitter and extractor.

The emitter and propellant tank are encased in a stereolithography 3D printed body which was manufactured out of Formlabs Rigid Resin, procured through Protolabs Hubs. 3D printing was selected resulting from the need to place a heater within the thruster body. The thruster body consisted of three separate components which were the main body, the insert and the back. The main body contains the square-shaped hole in which the emitter and propellant tank are aligned. It also contains grooves for the heater and holes for thermocouples to be placed in. The insert also contains grooves for the heater. The back of the body contains the hole for which the resevoir bolt is attached through. The three body components are tightly attached via four bolts, which connect the body with the extractor.

Heating is provided by a Thermocoax heater which is a wire with a 1.10 mm diameter which is made up of three layers: the central conductor, a ceramic insulation layer and metal shielding on the outside. Alongside maintaining a large resistance, meaning less current is required to control the heater, the heater is insulated. This means that if there is leakage of propellant, the heater will not short with the emitter and prevent damage to the sensitive control equipment.

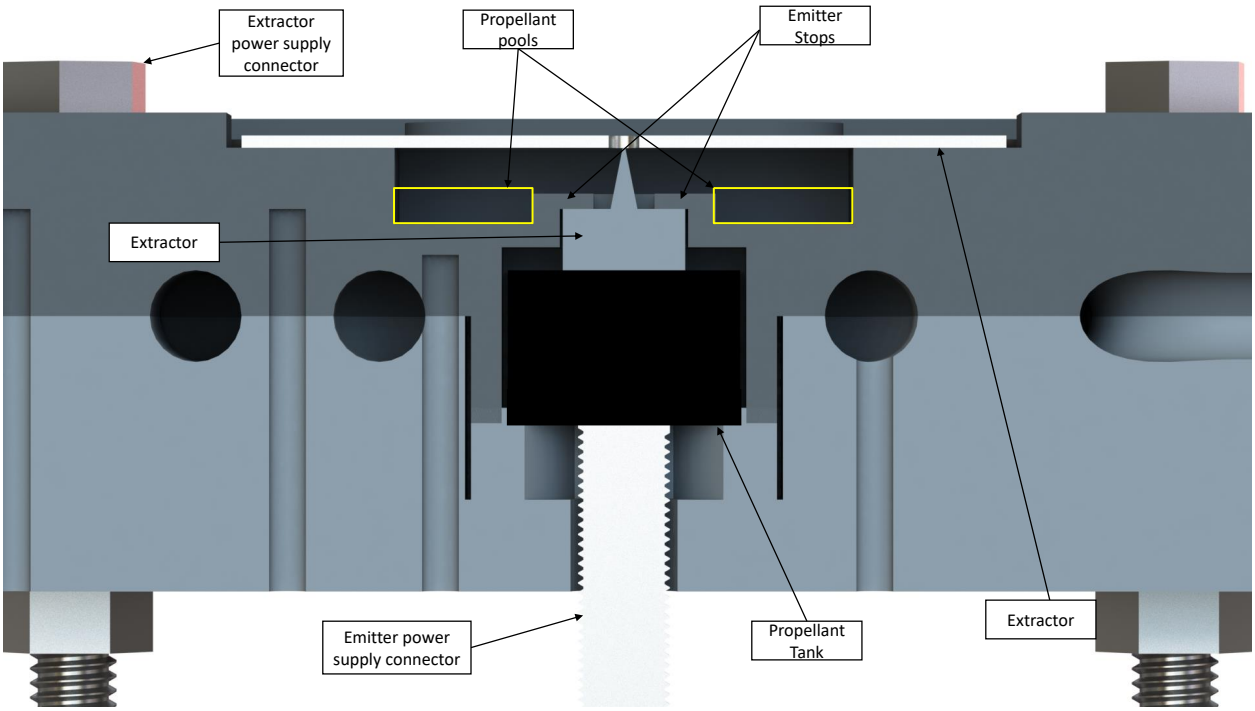

Fig. 1 The cut-out diagram of the HPET-1 showing the major PET features. The vertical holes are for thermocouples and the horizontal circulars are for the wire heater.

Fig 1 shows a cut-out of the HPET-1. The alignment of the emitter, resevoir and emitter bolt are shown. The dark grey and light grey show the thruster main body and the thruster insert respectively. Propellant pools were included in the design to increase the path length between the emitter and extractor so that any pooling EMI-BF4 would be less likely to cause an end-of-life short. Emitter stops were used to ensure alignment between the emitter and extractor. Due to plume impingement, the extractor in the latest iteration was moved to be on axis with the thruster. However due to a manufacturing error, the test thruster had a extractor displacement of 0.5 mm.

Fig. 2 shows the rear and front of the thruster. Fig. 2(a) shows the back of the thruster with with the back holder removed. The propellant tank can be seen in the thruster. The black plate has a slot for a nut which the rear bolt is threaded through. Furthmore, thermocouple holes can be seen on the back plate. Fig 2(b) shows the front of the thruster once it has been fully assembled. Three of the extractor mounting bolts use a ceramic spacer to insulate them from the extractor, while one of them is directly connected to the extractor to provide an electrical connection.

The heater was controlled by two K-type thermocouples, one placed directly on the heater and a second one placed in an orifice in the main body 1.00 mm away from the emitter. The heater was controlled by a LabVIEW On/Off program, where when the temperature exceeded the set temperature, the heater would turn off. This was found to provide good temperature control for such low temperatures, with a steady-state temperature range of +/- 1.0^{o}C around the set temperature. A further two K-type thermocouples were used, which would provide the temperature range across the thruster body. A National Instruments DAQ system was utilised to collect the thermocouple temperature and send a signal to a custom-made control circuit to control the heater.

III. Experimental Apparatus & Methods

A. Experimental Apparatus

The HPET-1 was tested at the David Fearn Electric Propulsion Labratory at the University of Southampton. The 'Hatch' chamber was used, which is a 0.70 m radius by 0.70 m cylindrical vacuum chamber. This chamber uses an Edwards XDS 35i scroll pump for roughing and an Oerlikon Leybold MAG W 700 iP turbopump, being able to bring the vacuum pressure down to 1.5×10^{-5} mBar during normal operation.

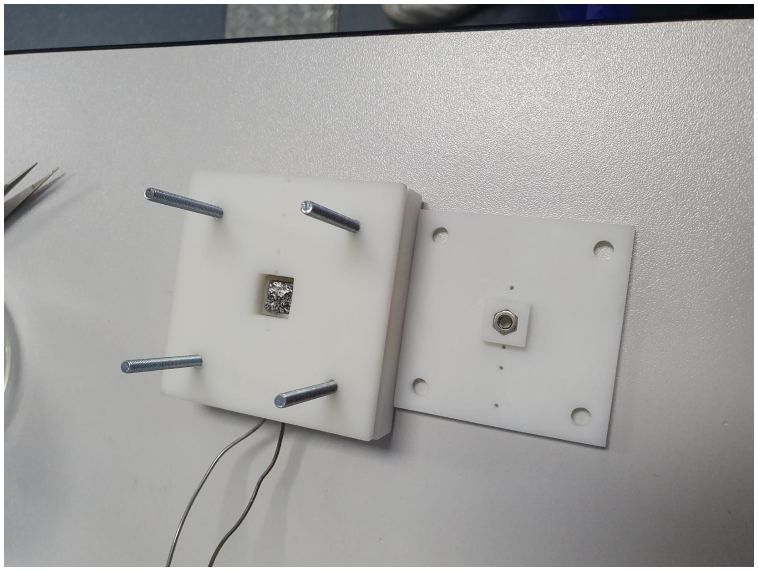

(a) The rear of the HPET-1.

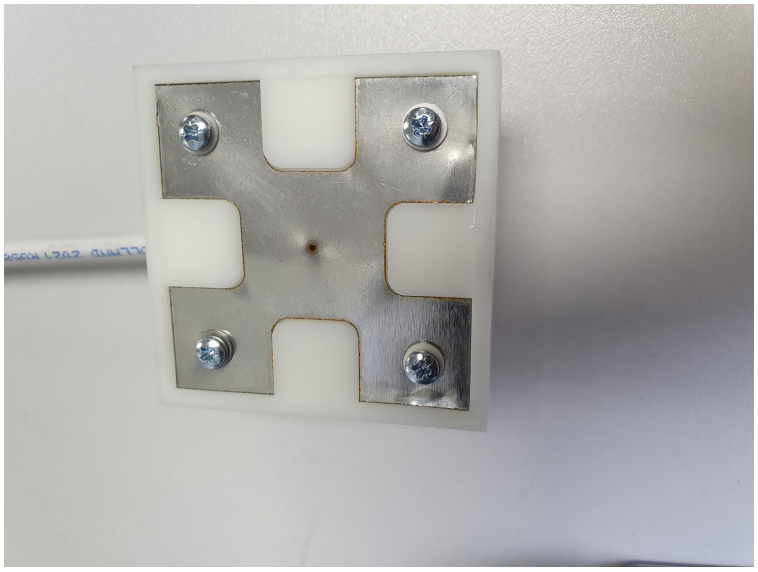

(b) The front of the HPET-1.

Fig. 2 Two pictures showing the assmebled HPET-1 prior to testing.

The voltage supplied to the emitter was provided by either two FuG Eletronik HCP-35-3500 power supplies which were set to the same voltage however at different polarities. The voltage was alternated by an in-house manufactured switching box, which utilised a square wave signal from a function generator to switch a relay. For retarding potential analysis testing, a Matsusada programmable power supply applied the retarding voltage, with the voltage supplied controlled by a LabVIEW program.

The thruster was placed on an in-house manufactured made rotary stage which was located in between a current collector and a retarding potential analyser. This allowed for either full plume current collection or, through rotating the thruster, retarding potential analysis and plume angle analysis. The rotary stage was controlled using an arduino motor driver which used an arduino program. The angle to be rotated was input into the program and the thruster would proceed to rotate by the amount clockwise, followed by immediately rotating anti-clockwise. The voltage applied to the rotary stage was recorded and the angle rotated was calculated using the amount of steps.

The current collector was made out of molybdenum and had a MN-17 nickel grid placed 5 mm above the plate to

supress Secondary Electron Emission effects by applying a -80V potential to the grid. The current collected by the plate was recorded by a Femto DHPCA-100 Fast Amp, which was connected to a Picoscope 2202 digital oscilloscope. This was connected to a computer to record the data. Furthermore, the extractor current was collected in the test using a 0.9094 MΩ resistor, which was connected to the extractor and then to the ground. The voltage produced by the current was recorded manually using a multimeter.

The retarding potential analyser was also manufactured in-house. The retarding potential analyser consists of three grids: a secondary electron emission supression grid, a retarding grid and a grounded grid. The retarding grid changes potential from 0 V up to emitter potential, preventing any particles with energy less than the retarding potential to be measured. Finally, the grounded grid is placed furthest away to terminate the electric field. The distance between each grid is 5 mm. The current collected by the retarding potential analyser was recorded by an in-house built LabVIEW DAQ system. It was placed 115 mm away from the thruster.

B. Methodology

Before testing, the thruster underwent a preparation procedure. Firstly, the emitter and the porous resevoir were submerged in EMI-BF4 in a beaker. This beaker was then placed in a vacuum chamber and brought down to roughing pressure ($\sim 5.0\times10^{-2}$ mBar) and left in the chamber over night. The next day, before testing, the three body components and the extractor were washed using isopropyl alcohol. The components were then dried to ensure that no liquid remained in the vacuum chamber. The thruster was then assembled, with the emitter and propellant tank being placed into the main body first and any excess EMI-BF4 being wiped off the thruster body. Finally, the thruster would be assembled and mounted on the rotary stage. Between removing the emitter and propellant tank from the vacuum chamber and the thruster being mounted and roughed down, the procedure took approximately one hour. The procedure was conducted at this pace mitigate any water absorption from the atmosphere.

Three tests were conducted on the HPET-1. These were the Current-Voltage-Temperature testing, Plume Angle Analysis and Retarding Potential Analysis. For the Current-Voltage-Temperature tests, voltage and temperature were varied to see the change in current. Firstly, the thruster's temperature was set to a given value. Once the heater had risen and settled to the required temperature, the testing would begin. The onset voltage was first found by increasing the voltage until the thruster began emitting. Then the voltage would be kept at the voltage for 5 minutes. After this, the voltage would be slowly decreased until emission ceased. The voltage sweep would occur from the nearest 100 V multiple of the onset voltage. The voltage would then been increased in increments of 100 V until the extractor current exceeded 2 μA. The voltage was then incremented down, until emission ceased. The temperature was increased in increments of 10^{o}C up to 80^{o}C and then decreased back to room temperature. A voltage sweep was conducted at each temperature.

Plume angle analysis followed a similar methodology. Initially, the temperature was maintained at the room temperature. The thruster's voltage was increased until it emitted stably. The thruster was kept unipolar throughout testing only for plume angle analysis and retarding potential analysis. Then the rotary stage was rotated by 180^{o} clockwise, immediately followed by rotating 180^{o} anti-clockwise to return to its position. Throughout the rotation, the retarding potential analyser, acting as a faraday cup, recorded the current collected continuously. As with the Current-Voltage-Temperature testing, a voltage sweep was first completed, before the temperature was increased and a further voltage sweep was done. The thruster was intially operated at 25^{o}C and then increased to 40^{o}C, 60^{o}C and 80^{o}C.

Finally, for the retarding potential analysis, a similar methodology was followed. Firstly, the thruster was aligned to the retarding potential analyser so that the extractor and the retarding potential analyser were coaxial and the retarding potential analyser had a 115 mm displacement from the thruster. The temperature was set initially to 40^{o}C. The voltage of the thruster was then increased until it emitted stably in unipolar mode. To conduct the votlage sweep, the Matsusada power supply was programmed to sweep the voltage linearly between 0 V and 5000 V, the maximum voltage of the power supply, over a period of 10 seconds. The voltage was then kept at 5000 V for 10 seconds. Finally, the voltage decreased linearly from 5000 V to 0 V over a period of 10 seconds. This was repeated once. The voltage was then swept in increments of 200 V and the temperature was swept in increments of 20^{o}C, up to 100^{o}C. Fig. 3 shows a picture of the HPET-1 mounted on the rotary stage with the current collector and the retarding potential analyser before testing.

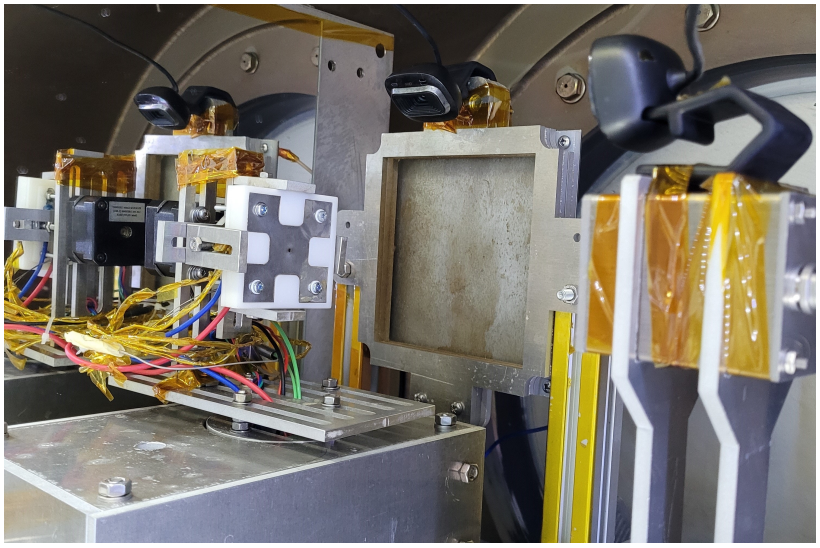

Fig. 3 The HPET-1 inside of the chamber mounted on the rotary testing system. On the left is that current collector. Closest to the camera, on the right is the retarding potential analyser.

IV. Results & Discussion

A. Current Collection

The thruster was found to onset at a varying voltage between 2.13 kV and 2.30 kV at varying temperatures, decreasing as the temperature increased. The transient data shown in Fig. 4 shows the current recorded as the thruster's emitter voltage was increased. Initially, as the voltage is close to the onset voltage, the thruster emits small amount of charge over small periods of time. As the thruster voltage is increased, the thruster still emit charge only periodically, however the period of time in between charge emission is decreased. Finally, the thruster reaches stability where the current is emitted in a square wave which is the same as the supplied bipolar voltage waveform.

To calculate the current emitted for a given temperature and voltage, a method for attaining the current would have to be used to mitigate for transient behaviour. Firstly, the charge of a given emission can be calculated by calculating the area of each emission:

$$Q = \int I(t)dt \tag{1}$$

Where Q is the emitted current per emission and $I(t)$ is the current measured by the current collector. This was calculated programmatically using the Trapezium rule. For multiple discharges, such as in Fig. 4 (b), the total charge would be calculated by summing the area of n discharges:

$$Q_{emission} = \sum_{i=1}^{n} Q_i \tag{2}$$

Where $Q_{emission}$ is the total emission current. Finally, to calculate the current, the total charge is divided by the period of the square wave. τ, which was set to 5 seconds throughout testing:

$$I = \frac{Q_{emission}}{\tau} \tag{3}$$

Using this method, the current for each voltage and temperature point was calculated. Furthermore, the current experiment was repeated four times, where two readings were taken on one day with two more taken the day after and the readings were averaged. The standard deviation between the readings was taken as the error. The extractor current and the collected current were summed to provide a total emission current. The total current for all voltages and temperatures is shown in Fig. 5. The raw data, with the error bars, can be found in Appendix A.

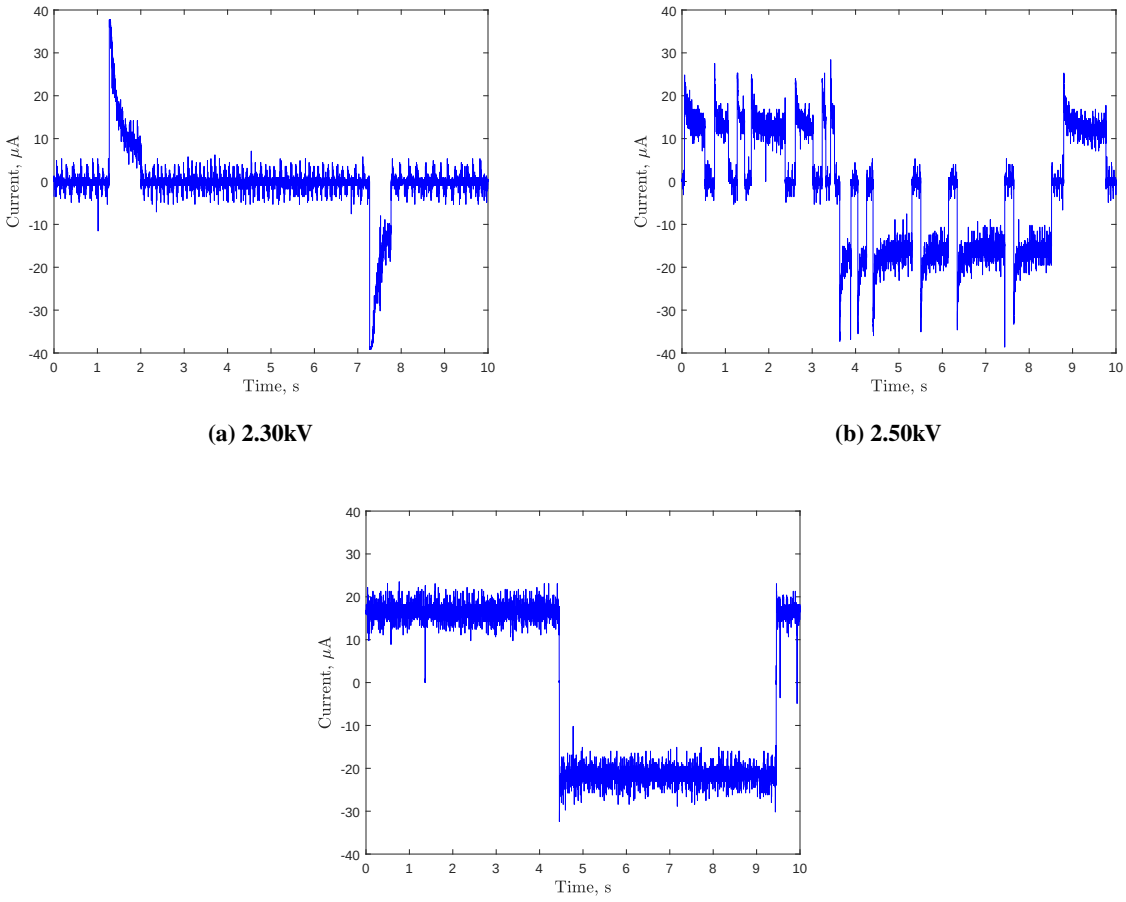

(a) 2.30kV

(b) 2.50kV

(c) 2.70kV

Fig. 4 Three graphs showing the change in transient behaviour at 40°C over a voltage range of 2.30kV to 2.70kV.

It can be seen that the current increases with voltage and temperature, which is expected of a PET. As voltage increases, the electric field strength increases within the PET, extracting more ions. Secondly, as the temperatures increases, the propellant properties change, especially conductivity. At a temperature of 80°C, the conductivity increases by approximately a factor of 5 compared to the conductivity at 25°C. The current density of a thruster emitting ions can be modelled by:

$$j = \sigma \frac{k_b T}{h} \; exp\left(-\frac{\Delta G - G_e}{k_b T}\right) \tag{4}$$

Where j is the current density on the surface of the propellant, σ is the charge density on the surface of the propellant, k_b is the Boltzmann's constant, h is Planck's constant, T is the temperature of the propellant, ΔG is the activation energy of EMI-BF4 (1 - 2 eV) [23] and G_e is the reduction in the activation energy of the propellant, which can be represented by:

$$G_e = \sqrt{\frac{q^3 E}{4\pi\epsilon_0}} \tag{5}$$

Where E is the electric field strength and ϵ_0 is the permittivity of free space. Eq. 4 shows that as the potential applied on the emitter increases, E increases hence G_e increases, increasing the current density at the emitter tip. Secondly, considering the charge transport within the thruster, the current density can be defined using Ohm's Law:

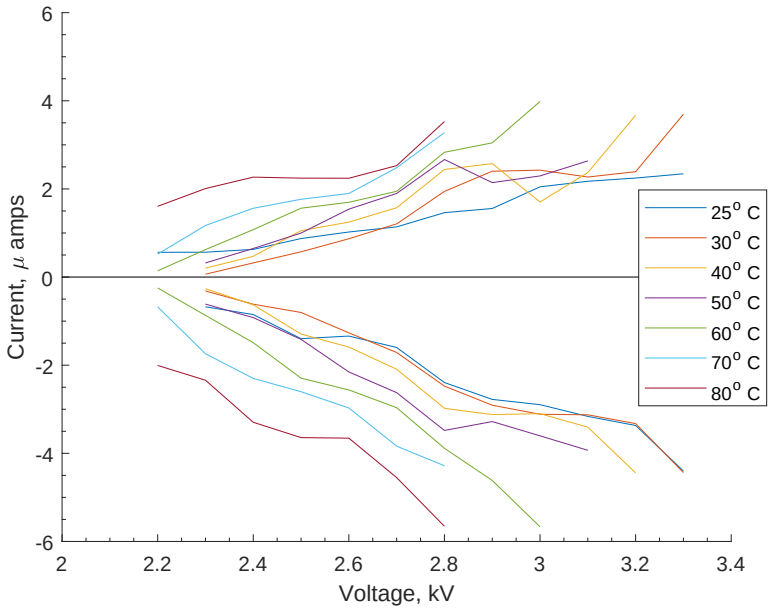

Fig. 5 The current emitted by the HPET-1 in operation. The data shows that the current increases for the same voltage as the temperature increases.

$$j = KE^i \tag{6}$$

Where K is the propellants conductivity and E^i is the internal electric field. It can be seen that $j \propto K$, therefore it is expected that as the temperature is increased, the current density, hence current, increases. As shown by Gassend *et al* [20] the current is expected to follow a linear increase in current output due to the limiting effect of the resistance of the propellant on the flow of charge. This is represented well in the data presented here and in other temperature work, such as by Krejci and Lozano [18].

B. Plume Angle Analysis

During plume angle testing, two difficulties were found which made the plume angle data unreliable. Firstly, the rotary stage used in testing was not supplied with voltage constantly and was also not geared. This meant that the thruster would rotate due to the tension in the wiring if perturbed from rest. As testing continued, the thruster became continuously more misaligned with the retarding potential analyser. However, the plumes of the thruster were able to be extracted, assuming that the plume of the thruster was centered at the centre of the plume. Furthmore, the measuring system would periodically short due to the motor leading to large amounts of noise.

Secondly, it is likely that the extractor heavily impinged throughout testing. The half-angle of the thruster throughout testing increased from 10^o to 20 ^{o} and remained at 20^o. Previous work on porous electrospray thrusters suggests a much higher angle is suitable for porous electrospray thrusters, exceeding 30^o [18, 24, 25]. This suggests that the half-angle recorded is lower than expected.

With the extractor being placed 0.5 mm away from the thruster with a aperture diameter of 1.0 mm that maximum half-angle possible is 45^o. This is much larger than the report 20^o report and suggests that beam impingement is not the cause of the lower plume half-angle. One possible resolution is a manufacturing error, creating an electric field which skews the beam towards the extractor or reduces the aperture size. However a manufacturing error would more likely increase the aperture size due to the hole being drilled out. Furthermore, the aperture would have to have a diameter of 0.47 mm for the correct size for impingenement, also being unlikely.

Another reason could be that the singular emitter geometry leads to a lower half-angle of the thruster. Due to the high noise experienced in the data, the trends were difficult to discern and further work is required to discern the cause

of the low angle.

Fig. 6 shows two of the profiles collected at 2.90 kV and 40°C at positive and negative current. The plumes show a rough approximation of a standard distribution of the plume, although Fig. 6 (a) is also flattened at the top, suggesting a less standard plume. Further analysis of the plume, looking at the change in plume angle of the thruster against temperature and voltage was made impossible due to the aformentioned problems and therefore is not looked at here, but will be an area of improvement for future tests.

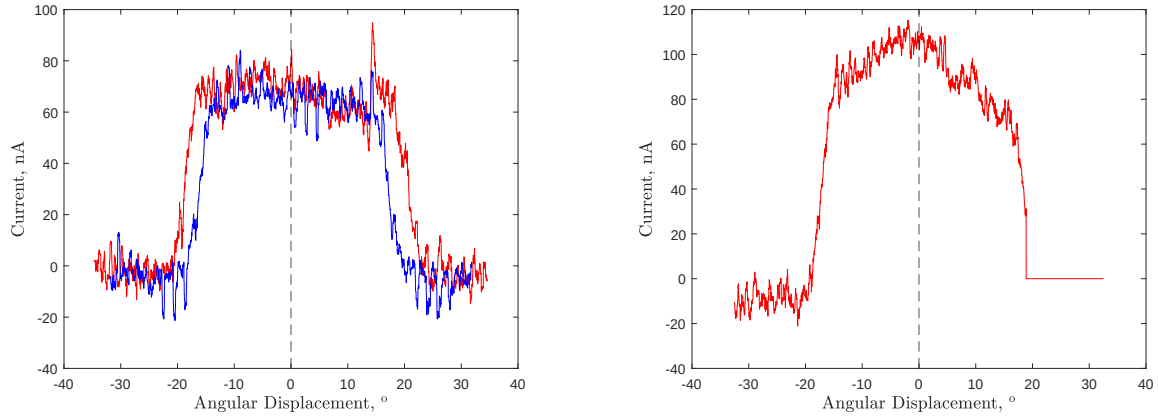

(a) Positive Current. **(b) Negative Current.**

Fig. 6 Two profiles of the thruster at 40°C and 2.90 kV showing positive and negative current. The profiles are clipped at the tails due to the extractor being 0.5 mm away.

C. Retarding Potential Analysis

The final test conducted on the thruster was retarding potential analysis. Firstly, it was assumed that the plume consists of only monomers and dimers. This is based off previous work completed at the University of Southampton [12]. The shape of the energy curves, of which a selection can be seen in Appendix B, show three regions, one drop of current at 0.359 or 0.305 the emitter potential which corresponds to the fragmentation of positive and negative dimers respectively in the Field Free Region (FFR). Secondly, there is a linear decrease in the current between 0.305/0.359 and slightly less than the emitter potential. This corresponds to fragmentation in the Acceleration Region (AR) [14]. Finally, at around the emitter potential, the current drastically drops to 0. This corresponds to the emitted monomers and unfragmented dimers. This can be seen in Fig. 7.

Miller [26] also calculated that in the near emitter electric field of an emitter, a significant proportions of dimers of EMI-Im and EMI-FAP will fragment with very little energy, producing monomers which look identical to unfragmented monomers in energy, however which produce a neutral fragment. It is expected that this pattern will be similar for EMI-BF4, as the mean lifetime of EMI-BF4 was shown to be lower than EMI-FAP [26] hence were more likely to fragment. Due to this effect, the proportion of the current which is calcuated at energy of approximately the emitter voltage is termed 'Current Accelerated to Maximum Potential' rather than the 'Unfragmented Current'. This is because the instrumentation used within this experiment cannot discern between unfragmented monomers and dimers and very low energy fragmented dimers. Fig. 7 shows the three different ratios on a graph of the raw RPA data.

The axis of the graphs are represented by the relative voltage and relative current, $\hat{V}$ and $\hat{I}$ respectively. These were calculated using the formula:

$$\hat{V} = \frac{V(t)}{V_{emitter}} \tag{7}$$

$$\hat{I} = \frac{I(V) - I_{offset}}{I_{max}} \tag{8}$$

Where $V(t)$ is the retarding voltage applied at a given time, $V_{emitter}$ is the emitter voltage, $I(V)$ is the collected current for a given retarding voltage, I_{offset} is an offset current produced by the measurement instrument and I_{max} is the maximum current recorded, when there $V(t) = 0$. Fig. 7 shows the regions in which each current ratio was calculated. Due to offsets in the current collection instruments, the relative currents at $\hat{V} = 0$ and $\hat{V} = 1$ occasionally were greater than $\hat{I} = 1$ and lower than $\hat{I} = 0$. For these points a correction formula used to ensure the ratios summed to 1:

$$I_r = \frac{\hat{I}_1 - \hat{I}_2}{\hat{I}_{max} - \hat{I}_{min}} \tag{9}$$

Where I_r is that calculated ratio, $\hat{I}_1$ and $\hat{I}_2$ are the relative currents bounding the ratio and $\hat{I}_{max}$ and $\hat{I}_{min}$ are the maximum and minimum relative current value for the energy curve respectively. One problem with the offset current was that it could change throughout testing, and this would cause the current to 'short', which can be seen in Appendix B Fig. 10 (b). For most curves, this would still allow for the calculation of the current ratios, however occasionally important turning points would 'short' and therefore some data was discarded.

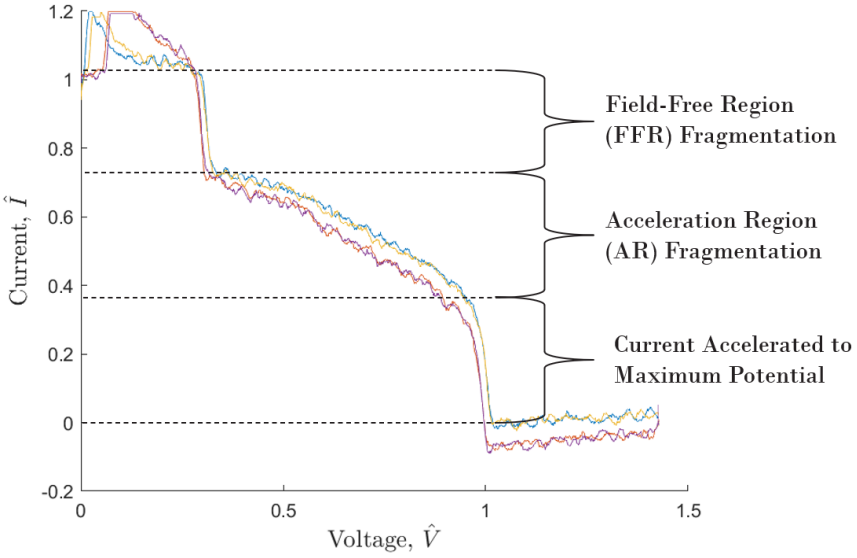

Fig. 7 A graph showing how each current ratio was calculated. The FFR, AR and Current Accelerated to Maximum Potential ratio are highlighted on the graph of raw retarding potential analysis data. The energy profile was taken up to eight different times for each voltage and temperature point.

Fig. 8 shows the calculated proportions of current in each region of the thruster for each temperature and voltage. Fig 8 (a)-(b) show that the plume of the thruster had high levels of current accelerated to emitter potential, with 30% to 65% of the current being accelerated to maximum potential. This showed a weak inverse relationship voltage, with the higher voltages decreasing the proportion of the current being accelerated to maximum potential. A stronger relationship was seen with temperature, with a higher temperature increasing the ratio of current which was accelerated to maximum potential.

Fig. 8 (c)-(f) shows the fragmentation ratios in the AR and FFR respectively. These ratios seemed to indicate no pattern with temperature or voltage, which was anomalous as it is expected that an increase in temperature will increase the ratio of fragmented current, while an increase in voltage should increase the fragmentation within the acceleration region. This can be modelled considering that the fragmentation rates can be modelled by an Arrhenius type equation[16]:

$$r = A \exp\left(-\frac{E_{frag} - \Delta E_{frag,e}}{k_b T_i}\right) \tag{10}$$

Where r is the rate of fragmentation of the species, A is an empirical constant, E_{frag} is the energy barrier for fragmentation ($\sim$ 1 eV) , which is assumed to be similar to 1- ethyl-3- methylimidazolium tris(pentafluoroethyl)trifluorophosphate

(EMI-FAP) and 1,2-dimethyl-3-propylimidazolium-methide (DMPI-Me) which was measured by de la Mora[27], $\Delta E_{frag,e}$ is the energy reduction in the fragmentation energy due to the presence of an electric field (calculated as in Eq. 5) and T_i is the ion temperature (O ~ 10^2 K). The ion temperature was calculated be rearranging Eq. 10 for T_i and calculated using the specified parameters [16]. Using this equation, it is expected that as the voltage is increased, the reaction rate of dimers will increase. This implies that fewer dimers will arrive unfragmented therefore the collected current which is accelerated to the potential will be lower. This is reflected in the current accelerated to emitter potential ratio. However, in the AR fragmented current ratio and FFR fragmented current ratio, there is no relationship in voltage.

For the temperature relationship, a trend is suggested in the current accelerated to emitter potential, as an increase in the temperature increases the ratio. This could suggest that either more dimers are fragmenting in the near emitter region, then being accelerated to maximum potential, or that the current emitted contains more monomers which then remain unfragmented. It is likely that the latter is true, as Eq. 10 suggests that the reaction rate increases as the temperature increases. Furthermore, Time-of-Flight experiments showed that an increase in temperature increases the ion proportion in the plume [20]. As with the voltage, no clear pattern is indicated by the proportions of FFR and AR fragmentation for temperature as well.

One interesting aspect of the collected data is at 60°C the current accelerated to maximum potential ratio is higher than at any other point, anomalous to every other temperature collected. This can be seen in Fig. 8 (a) and (b) but also (c) - (f). This can be seen somewhat in work by Miller where the mean lifetime for EMI-BF4 seemed to seemed to be higher for 60°C than for 40°C [16]. This would suggest that that either at this temperature proportionally more monomers are emitted or that dimers are less likely fragment and therefore more dimers arrive at the collector. The latter option seems unlikely, as this would go against common knowledge about fragmentation. The former option would suggest

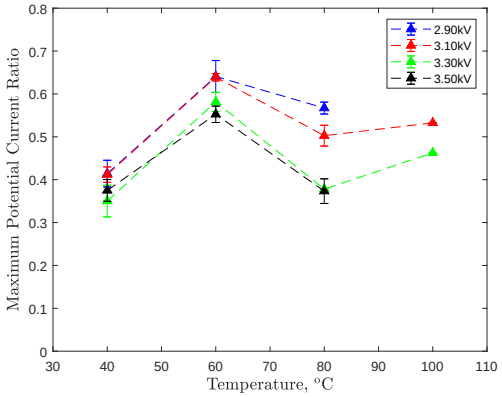

(a) The temperature dependence of the unfragmented current for the anions.

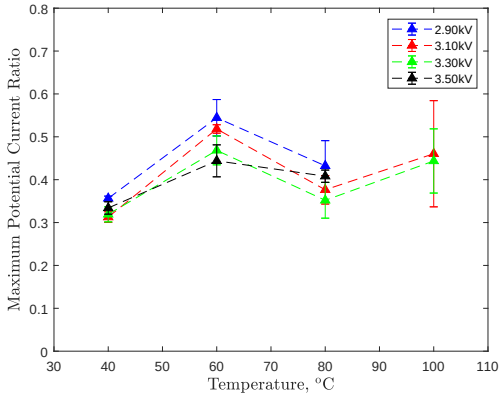

(b) The temperature dependence of the unfragmented current for the cations.

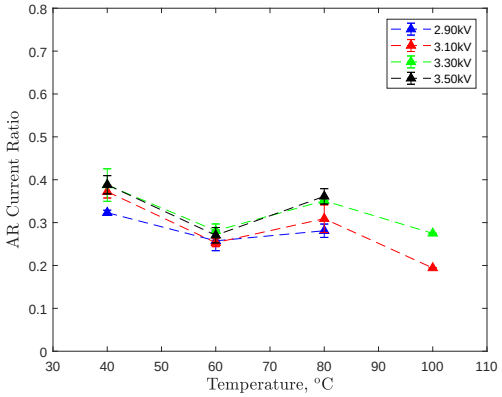

(c) The temperature dependence of the fragmented current in the AR for the anions.

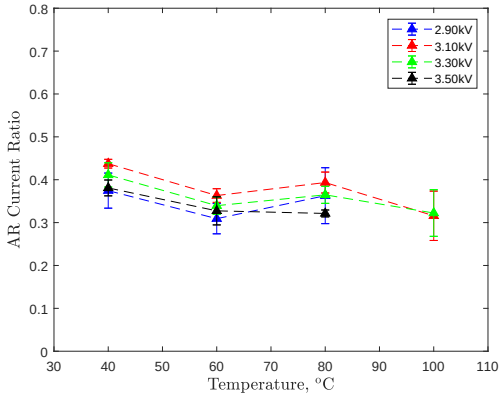

(d) The temperature dependence of the fragmented current in the AR for the cations.

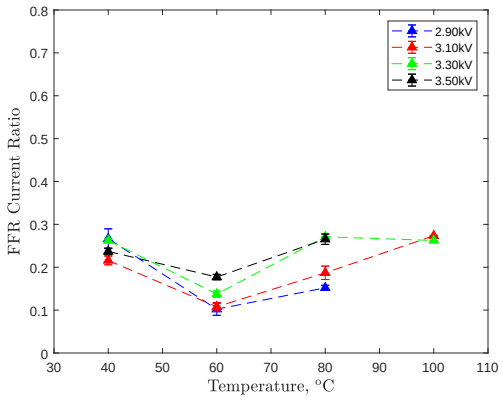

(e) The temperature dependence of the fragmented current in the FFR for the anions.

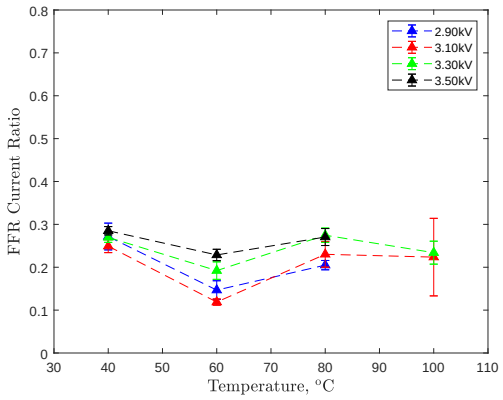

(f) The temperature dependence of the fragmented current in the FFR for the cations.

Fig. 8 A series of graph showing the voltage and temperature dependence on the fragmentation ratios in the three different regimes of a PET: current accelerated to maximum potential, fragmentation in the AR and fragmentation in the FFR. It can be seen that the increasing the temperature and voltage decreases the unfragmented current ratio. However at 60°C it is found that the current is anomalously less fragmented than for the other temperatures.

interesting emission phenomena causing more monomer emission in the plume. Currently, the anomalous increase in energy at 60°C is treated as an instrumentation error however further work is required to confirm these readings.

One issue through testing was due to the large beam impingement seen by the thruster, the thruster shorted when testing at 100°C. This meant that further testing was not possible and hence only two readings were taken at 100°C. This will be alleviated by moving the extractor to the same plane as the emitter tip in the latest iteration of the design.

V. Conclusion

A heated porous electrospray thruster is presented, with its design described. The experiment methodology is presented for three experiments: current collection, plume angle analysis and retarding potential analysis. The current emitted by the thruster is presented, showing the thruster emitting between 3.9 μA to -5.9 μA with increasing temperature and voltage increasing the current. Plume angle analysis showed that plume half angle of the thruster is between 10° and 20°, however this is discerned to be due to the extractor being far away. Finally, the energy data of the plume is presented, showing a fully accelerated current ratio of 30% to 70%. Futhermore, it is shown that increasing the voltage seems to reduce this ratio and increasing the temperature increases this ratio, suggesting higher fragmentation and more monomer emission respectively.

Appendix A: Current data for each Temperature

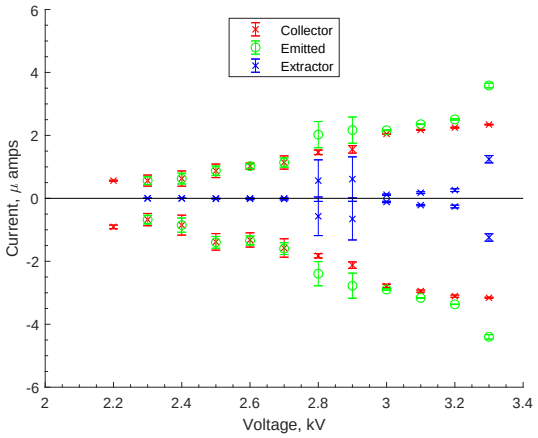

(a) 25°C

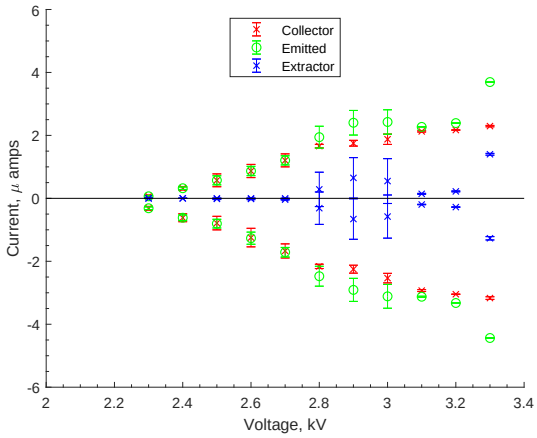

(b) 30°C

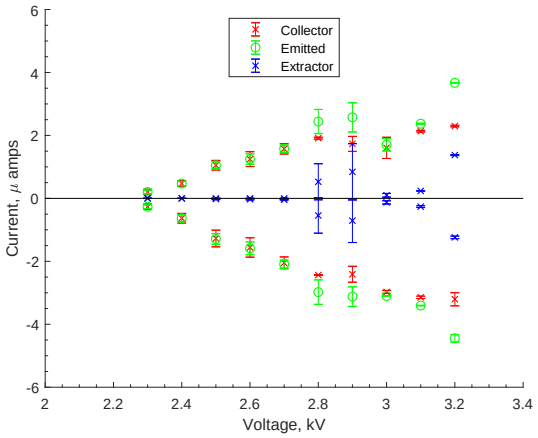

(c) 40°C

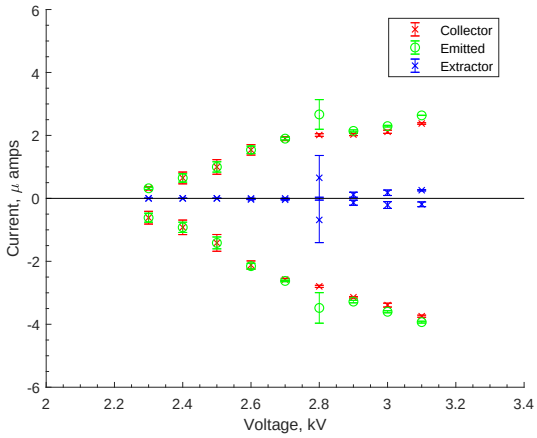

(d) 50°C

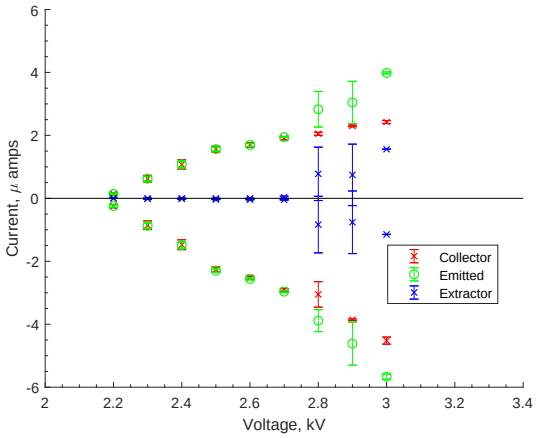

(e) 60°C

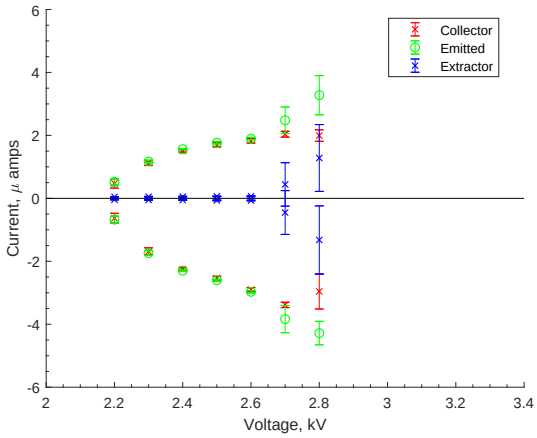

(f) 70°C

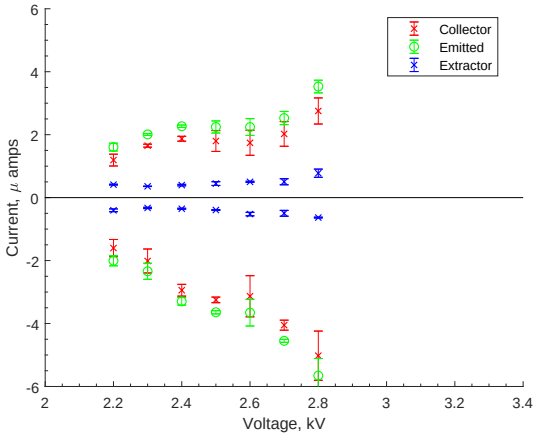

(g) 80°C

Fig. 9 The graphs showing the collector, extractor and emitted current for (a) 25°C, (b) 30°C, (c) 40°C, (d) 50°C, (e) 60°C, (f) 70°C and (g) 80°C.

Appendix B: Raw Retarding Potential Analysis Data

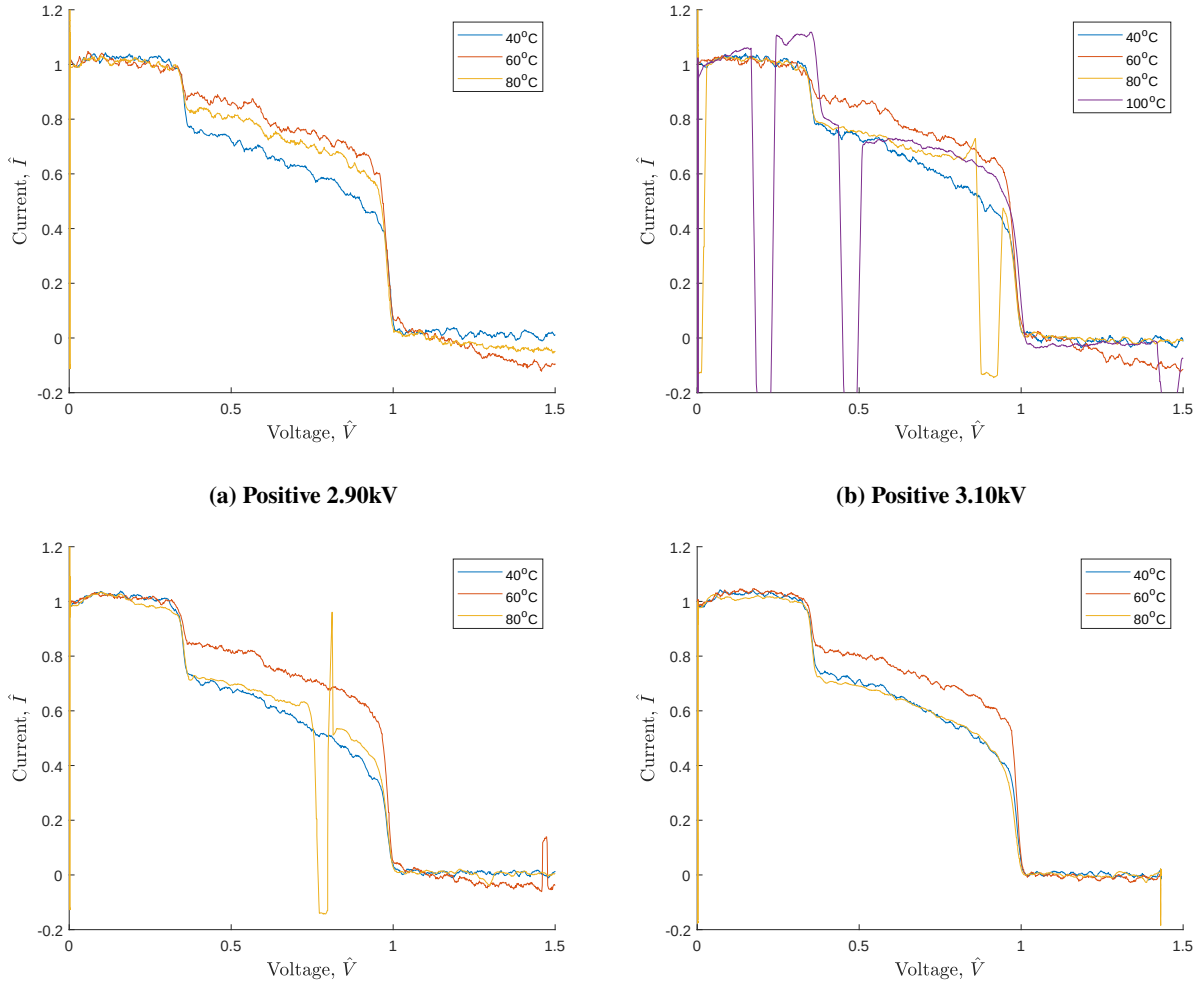

(a) Positive 2.90kV

(b) Positive 3.10kV

(c) Positive 3.30kV

(d) Positive 3.50kV

Fig. 10 The RPA data for the positive polarity from 2.90kV to 3.50kV. Due to thruster instability, 100°C was only recorded for 3.10kV. Shorting occured during testing and can be seen in (b) and (c).

References

[1] Villela, T., Costa, C. A., Brandão, A. M., Bueno, F. T., and Leonardi, R., "Towards the thousandth CubeSat: A statistical overview," *International Journal of Aerospace Engineering*, Vol. 145, No. 24, 2019, pp. 44–46.

[2] Lemmer, K., "Propulsion for CubeSats," *Acta Astronautica*, Vol. 134, 2017, pp. 231–243.

[3] Taylor, G. I., "Disintegration of water drops in an electric field," *Proceedings of the Royal Society of London. Series A. Mathematical and Physical Sciences*, Vol. 280, No. 1382, 1964, pp. 383–397.

[4] Taylor, G. I., and McEwan, A. D., "The stability of a horizontal fluid interface in a vertical electric field," *Journal of Fluid Mechanics*, Vol. 22, No. 1, 1965, p. 1–15.

[5] De La Mora, J. F., and Loscertales, I. G., "The current emitted by highly conducting Taylor cones," *Journal of Fluid Mechanics*, Vol. 260, 1994, pp. 155–184.

[6] Loscertales, I. G., and Fernández de la Mora, J., "Experiments on the kinetics of field evaporation of small ions from droplets," *The Journal of Chemical Physics*, Vol. 103, No. 12, 1995, pp. 5041–5060.

[7] Romero-Sanz, I., Bocanegra, R., Fernandez de la Mora, J., and Gamero-Castaño, M., "Source of heavy molecular ions based on Taylor cones of ionic liquids operating in the pure ion evaporation regime," *Journal of Applied Physics*, Vol. 94, No. 5, 2003, pp. 3599–3605.

[8] Coffman, C., Martínez-Sánchez, M., Higuera, F. J., and Lozano, P. C., "Structure of the menisci of leaky dielectric liquids during electrically-assisted evaporation of ions," *Applied Physics Letters*, Vol. 109, No. 23, 2016, p. 231602.

[9] Mehta, N. A., and Levin, D. A., "Molecular Dynamics Electrospray Simulations of Coarse-Grained Ethylammonium Nitrate (EAN) and 1-Ethyl-3-Methylimidazolium Tetrafluoroborate (EMIM-BF4)," *Aerospace*, Vol. 5, No. 1, 2018.

[10] Courtney, D. G., Dandavino, S., and Shea, H., "Comparing Direct and Indirect Thrust Measurements from Passively Fed Ionic Electrospray Thrusters," *Journal of Propulsion and Power*, Vol. 32, No. 2, 2016, pp. 392–407.

[11] Krejci, D., Mier-Hicks, F., Thomas, R., Haag, T., and Lozano, P. C., "Emission Characteristics of Passively Fed Electrospray Microthrusters with Propellant Reservoirs," *Journal of Spacecraft and Rockets*, Vol. 54, No. 2, 2017, pp. 447–458.

[12] Ma, C., Bull, T., and Ryan, C. N., "Plume Composition Measurements of a High-Emission-Density Electrospray Thruster," *Journal of Propulsion and Power*, Vol. 37, No. 6, 2021, pp. 816–831.

[13] Lozano, P. C., "Energy properties of an EMI-Im ionic liquid ion source," *Journal of Physics D: Applied Physics*, Vol. 39, No. 1, 2005, pp. 126–134.

[14] Ma, C., and Ryan, C., "Plume particle energy analysis of an ionic liquid electrospray ion source with high emission density," *Journal of Applied Physics*, Vol. 129, No. 8, 2021, p. 083302.

[15] Chong, C., Maolin, C., and Haohao, Z., "Characterization of an ionic liquid electrospray thruster with a porous ceramic emitter," *Plasma Science and Technology*, Vol. 22, No. 9, 2020, p. 094009.

[16] Miller, C. E., and Lozano, P. C., "Measurement of the dissociation rates of ion clusters in ionic liquid ion sources," *Applied Physics Letters*, Vol. 116, No. 25, 2020, p. 254101.

[17] Alexander Harrison, J., Pruška, A., Oganesyan, I., Bittner, P., and Zenobi, R., "Temperature-Controlled Electrospray Ionization: Recent Progress and Applications," *Chemistry – A European Journal*, Vol. 27, No. 72, 2021, pp. 18015–18028.

[18] Krejci, D., and Lozano, P., "Scalable Ionic Liquid Electrospray Thrusters for Nanosatellites," 2016.

[19] Gamero-Castaño, M., and Cisquella-Serra, A., "Electrosprays of highly conducting liquids: A study of droplet and ion emission based on retarding potential and time-of-flight spectrometry," *Phys. Rev. Fluids*, Vol. 6, 2021, p. 013701.

[20] Gassend, B., Velásquez-García, L. F., Akinwande, A., and Martínez-Sánchez, M., "A fully integrated microfabricated externally wetted electrospray thruster," *30th International Electric Propulsion Conference*, 2007.

[21] Stoppa, A., Zech, O., Kunz, W., and Buchner, R., "The Conductivity of Imidazolium-Based Ionic Liquids from (-35 to 195) ^{o}C. A. Variation of Cation's Alkyl Chain," *Journal of Chemical and Engineering Data*, Vol. 55, No. 5, 2010, pp. 1768–1773.

[22] Nuwal, N., Azevedo, V. A., Klosterman, M. R., Budaraju, S., Levin, D. A., and Rovey, J. L., "Multiscale modeling of fragmentation in an electrospray plume," *Journal of Applied Physics*, Vol. 130, No. 18, 2021, p. 184903.

[23] Guerrero, I., Bocanegra, R., Higuera, F., and De La Mora, J. F., "Ion evaporation from Taylor cones of propylene carbonate mixed with ionic liquids," *Journal of Fluid Mechanics*, Vol. 591, 2007, pp. 437–459.

[24] Natisin, M., Zamora, H., McGehee, W., Arnold, N., Holley, Z., Holmes, M., and Eckhardt, D., "Fabrication and characterization of a fully conventionally machined, high-performance porous-media electrospray thruster," *Journal of Micromechanics and Microengineering*, Vol. 30, No. 11, 2020, p. 115021.

[25] Ma, C., and Ryan, C., "Plume characterization of a porous electrospray thruster," *The 36th International Electric Propulsion Conference*, 2019, pp. 1–19.

[26] Miller, C. E., "Characterization of ion cluster fragmentation in ionic liquid ion sources," Ph.D. thesis, Massachusetts Institute of Technology, 2019.

[27] de la Mora, J. F., Genoni, M., Perez-Lorenzo, L., and Cezairli, M., "Measuring the kinetics of neutral pair evaporation from cluster ions of ionic liquid in the drift region of a differential mobility analyzer," *The Journal of Physical Chemistry A*, Vol. 124, No. 12, 2020, pp. 2483–2496.